HHS Public Access

Author manuscript

J Am Chem Soc. Author manuscript; available in PMC 2019 December 19.

Published in final edited form as:

J Am Chem Soc. 2018 December 19; 140(50): 17656–17665. doi:10.1021/jacs.8b09867.

Optical control of metal ion probes in cells and zebrafish using highly selective DNAzymes conjugated to upconversion nanoparticles

Zhenglin Yang[†,⊥], **Kang Yong Loh**[‡,⊥], **Yueh-Te Chu**[‡], **Ruopei Feng**[‡], **Nitya Sai Reddy Satyavolu**[‡], **Mengyi Xiong**[‡,‖], **Stephanie M. Nakamata Huynh**[‡], **Kevin Hwang**[‡], **Lele Li**[‡,§], **Hang Xing**[‡,‖], **Xiaobing Zhang**[‖], **Yann R. Chemla**[¶,#], **Martin Gruebele**[‡,¶,#], and **Yi Lu**[†,‡,¶,*]

[†]Department of Biochemistry, University of Illinois at Urbana-Champaign, Urbana, Illinois 61801, United States;

[‡]Department of Chemistry, University of Illinois at Urbana-Champaign, Urbana, Illinois 61801, United States;

[§]CAS Key Laboratory for Biomedical Effects of Nanomaterials and Nanosafety and CAS Center for Excellence in Nanoscience, National Center for Nanoscience and Technology, Beijing 100190, China;

[‖]Institute of Chemical Biology and Nanomedicine, College of Chemistry and Chemical Engineering, Hunan University, Changsha, Hunan 410082;

[¶]Center for Biophysics and Quantitative Biology, University of Illinois, Urbana, IL 61801, United States;

[#]Department of Physics, University of Illinois, Urbana, IL 61801, United States.

Abstract

Spatial and temporal distributions of metal ions in *vitro* and in *vivo* are crucial in our understanding of the roles of metal ions in biological systems, and yet there is a very limited number of methods to probe metal ions with high space and time resolution, especially in *vivo*. To overcome this limitation, we report a Zn^{2+}-specific near infrared (NIR) DNAzyme nanoprobe for real-time metal ion tracking with spatiotemporal control in early embryos and larvae of zebrafish. By conjugating photocaged DNAzymes onto lanthanide-doped upconversion nanoparticles (UCNPs), we have achieved upconversion of a deep tissue penetrating NIR 980 nm light into 365 nm emission. The UV photon then efficiently photo-decages a substrate strand containing a

[*]Corresponding Author: yi-lu@illinois.edu.
[⊥]These authors contributed equally.

Ethics Statement

All experimental procedures in this study were approved by the University of Illinois Institutional Animal Care and Uses Committee protocol #16080.

Supporting Information

The Supporting Information is available free of charge on the ACS Publications website at DOI:
Additional notes on fitting of kinetic data, characterization of seed and particles, and additional supporting figures of SEM and STEM images have been included. (PDF)

Notes

The authors declare no competing financial interests.

nitrobenzyl group at the 2'-OH of adenosine ribonucleotide, allowing enzymatic cleavage by a complementary DNA strand containing a Zn^{2+}-selective DNAzyme. The product containing a visible FAM fluorophore that is initially quenched by BHQ1 and Dabcyl quenchers, is released after cleavage, resulting in higher fluorescent signals. The DNAzyme-UCNP probe enables Zn^{2+} sensing by exciting in the NIR biological imaging window in both living cells and zebrafish embryos, and detecting in the visible region. This report introduces a platform that can be used to understand the Zn^{2+} distribution with spatiotemporal control, thereby giving insights into the dynamical Zn^{2+} ion distribution in intracellular and in vivo models.

INTRODUCTION

Metal ions play important roles in biological systems by stabilizing different conformations of biomolecules and by helping to catalyze many enzymatic functions.[1,2] It is well established that the identity and concentration of metal ions are different in different compartments of biological systems and that these distributions change with time.[3,4] Any abnormal distribution of metal ions can lead to various diseases including osmolarity imbalance, neural malfunction, and cancers.[5,6] Probing the distribution of these metal ions with high spatial and temporal resolution can offer unprecedented insight into how these metal ions help maintain health or cause diseases, and how they interact with therapeutics. Toward this goal, laser ablation inductively coupled plasma mass spectrometry (ICP-MS) and X-ray fluorescence (XRF) microtomography have provided high spatial resolution to probe metal ions *in vivo* such as zebrafish.[7–10] However, these methods rely on fixed or sliced biological tissues and thus cannot provide real time information about metal ion distributions with temporal resolution.

In the quest for spatiotemporal control of imaging *in vitro* and *in vivo*, photo-regulation research in the optogenetics field has proven to be a powerful method to control the timing and location of the function and detection of many biological molecules such as nucleic acids, proteins and biological cofactors.[11–13] However, due to their similar charges, atomic radii and chemical properties, most metal ions are much more difficult to probe selectively than nucleic acids and proteins. Therefore, there is a major demand for selective sensing or imaging probes for metal ions with high spatial and temporal control.

To overcome the challenge of optically controlling the detection of metal ions in biological systems, many metal ion sensors using small organic molecules, peptides or proteins have been developed,[14–21] and some of them have been applied in in vivo systems like zebrafish and mice.[22,23] However, only a limited number of these sensors allow optical control of the detection with both spatial and temporal precision to avoid unwanted early activation of the sensors *in vivo* and reduce nonspecific signals that hamper spatiotemporal specific imaging in living organisms. For those sensors that do display optical controls, the number of detectable metal ions is limited, and the method is difficult to generalize to be selective for other metal ions, and thus restricting the impact of the method on the understanding of biological roles of metal ions described above.

To address the lack of an optically controlled probe that can be generalized to many metal ions, a new class of metal ion sensors based on DNA molecules that display catalytic activity

(called deoxyribozymes or DNAzymes) was developed.[24–30] A major advantage of DNAzymes as metal ion sensors is that DNAzymes specific for almost any metal ion can be obtained from a large DNA library with up to 10^{15} different sequences, using a combinatorial process called *in vitro* selection.[31–33] Since the first publication on DNAzymes in 1994, many DNAzymes with specificity to Pb^{2+}, Mg^{2+}, Ca^{2+}, Cu^{2+}, Zn^{2+}, UO_2^{2+}, Cd^{2+}, Cr^{3+}, Ag^{+}, and Na^{+} have been isolated.[24,34–43] Furthermore, it is much easier to conjugate fluorophores and quenchers to these DNAzymes without sacrificing the metal binding affinity or selectivity, than to derivatize small organic molecules or proteins. As a result, we and others have developed the catalytic beacon approach to convert these DNAzymes into fluorescent sensors for both environmental monitoring and cellular imaging of metal ions.[44–46]

To achieve optical control of DNAzyme-based sensors for metal ion detection, we reported a photocaging/decaging strategy, by modifying the 2'-OH group of the RNA cleavage site with a 2'-nitrobenzyl group, protecting the substrate strand from cleavage until the cage is removed by 365 nm light.[47–50] However, the photodissociation of this protecting group by the 365 nm irradiation limits the applicability of this sensor to cellular and in vivo sensing, as the 365 nm light has poor penetration into tissue and can potentially cause phototoxicity to living cells or animals. To overcome this limitation, we became interested in lanthanide-doped upconversion nanoparticles (UCNPs), which are capable of converting near-infrared (NIR) excitation into shorter wavelength emissions absorbable by photocaging groups, and thus offering broad *in vivo* applications.[51–54] Given the deep tissue penetration abilities of NIR light, UCNPs have emerged as advantageous components of in vivo nanoprobes with the use of localized light sources in various bioimaging research and applications.[55,56] Therefore, by combining the high metal ion selectivity offered by DNAzymes and the deep tissue penetrating light excitation characteristics of UCNPs, DNAzyme-UCNP sensors have the potential to be a general method to allow optical control of detection of many metal ions with high temporal and spatial resolution in living cells and *in vivo*.

Herein, we report a NIR light controlled in vivo sensor for metal ions by conjugating a photocaged Zn^{2+}-specific DNAzyme to a NaYF4:Yb,Tm@NaYF4 UCNP that can convert 980 nm light into 365 nm emitting light (Figure 1a).[49,57] The substrate strand of the Zn^{2+} specific DNAzyme, named 8–17 DNAzyme, is protected from cleavage by modifying the 2'-OH of the scissile ribonucleotide adenosine (A) in the middle of a substrate strand with a 2'-nitrobenzyl group. This photocaged substrate strand is also conjugated with a carboxyfluorescein (FAM) fluorophore at the 3' end and Black Hole Quencher-1 (Q1) at the 5' end. Together with another Dabcyl quencher (Q2) incorporated at the 3' end of the enzyme strand, such a DNAzyme construct ensures complete quenching of the fluorophore upon hybridization of the two strands in the absence of Zn^{2+} and NIR light. Upon injection into zebrafish at the single cell stage, the construct can diffuse into all parts of the zebrafish without non-specific cleavage, even in the presence of Zn^{2+} and other species, because it is photocaged. When 980 nm light is applied to system, the UCNP can convert the NIR light into localized 365 nm emission, which is exactly the wavelength that can photo-dissociate the 2'-nitrobenzyl group from the substrate strand, restoring the 2'-OH and allowing highly Zn^{2+} specific cleavage of the single substrate strand into two shorter product strands. Because the melting temperature of the fluorophore-labeled cleavage product strand P2 and

the enzyme strand is designed to be below room temperature, at 14.7° C, the P2 strand dehybridizes from the enzyme strand, releasing the fluorescent moiety spatially away from the quenchers, resulting in a dramatic increase of the fluorescence signal. This deep penetrating NIR technique offers the control to activate the Zn^{2+} specific sensor in living organisms from embryonic stage to larval stage. Since the location and timing of the NIR light can be precisely regulated, we can achieve spatial and temporal optical control of the DNAzyme-UNCP system for detecting metal ions *in vivo* with higher penetration depth and much less damage than the more commonly used UV light.

RESULTS AND DISCUSSION

The photocaged Zn^{2+} specific 8–17 DNAzyme were synthesized and prepared as described previously.[49] To achieve 365 nm emission required to photo-decage this DNAzyme, we synthesized $NaYF_4$:Yb,Tm@$NaYF_4$ UCNP containing a 49:1 ratio of Yb:Tm with a diameter of ~ 32 nm (Supplemental Figure 1, 2). To realize the design shown in Figure 1a, we developed a novel multilayered functionalization method (Figure 1b) for quantum confinement and solvent isolation to enhance the quantum yield of the UCNP (Figure 2a). Specifically, the UCNP was coated with silica via a modified Stöber process.[58] The resultant silica coated nanoprobes were modified using (3-Aminopropyl)trimethoxysilane (APTMS) to yield exposed amine groups. This surface amine group was subsequently reacted with sulfosuccinimidyl 4-(N-maleimidomethyl)cyclohexane-1-carboxylate (Sulfo-SMCC) to covalently link to the maleimide groups, which are then conjugated to the thiol-modified DNA strands.[59] To minimize perturbation of the DNAzyme activity on the surface of UCNPs, we used a three-strand annealing method,[60] in which a thiolated linker DNA was first conjugated to the UCNP as described above and then hybridized to the 3’ portion of enzyme strand, while the substrate strand is hybridized to the 5’ portion of the enzyme strand. The progress of each step of the multilayer functionalization was monitored by FTIR characterization (Supplemental Figure 3) and by measuring Zeta potentials of the resulting UCNPs (Figure 2b). The average number of DNAzyme sensor molecules that have been conjugated on each UCNP is estimated to be 31. The final diameter of the DNAzyme-UCNP system was approximately 80 nm in size (Supplemental Figure 4), which was observed to have effective cellular uptake for imaging of metal ions *in vitro* and *in vivo* (Figure 3–5, Supplementary Figures 11–21).

We first tested the decaging kinetics of the above photocaged DNAzyme-UCNP by 365 nm light in the presence of Zn^{2+} and observed an increase of fluorescence signal with time (Figure 2c and d, Supplemental Figure 5). The performance remains similar to the photocaged DNAzyme before conjugation to the UCNP (Supplemental Figure 6, 7), indicating that the activity of this DNAzyme sensor is minimally affected by the UCNP conjugation steps. We then investigated the UCNP-based NIR decaging of the DNAzyme in PBS buffer at pH 7.0 by monitoring FAM emission at 520 nm before and after 980 nm irradiation. As shown in Figure 2e and f, compared with control sequences that could not be cleaved by Zn^{2+} DNAzyme, we observed an increase of fluorescence signal upon the NIR irradiation for 30 min in the presence of Zn^{2+}. These results indicate that the photo-protected substrate strand has been decaged and cleaved during this process. To further confirm the decaging efficiency by NIR irradiation compared with the published UV irradiation method,

we eluted DNA strands off from the UCNP surface after this *in vitro* activity assay and resolved these samples by polyacrylamide gel electrophoresis (PAGE). As shown in Supplemental Figure 8 and 9, the NIR decaging showed similar efficiency in decaging and cleaving the substrate strand as the UV decaging method, while no detectable amount of substrate was decaged and cleaved without light irradiation in the presence of the Zn^{2+} DNAzyme. Before the cellular work and zebrafish detection, we investigated the effect of Zn2+ concentrations on the performance of our DNAzyme-UCNP system and found that 100 μM Zn^{2+} gives the best results and thus was used for later experiments.

As the first step for intracellular studies, the cytotoxicity effect of the DNAzyme-UCNP system was assessed in HeLa cells using the MTT cell viability assay after incubating cells with the above DNAzyme-UCNP for 24 hours. The resultant data, shown in Figure 3a, indicated minimal toxicity. Since optical control is the critical step in our system, we tested cell viability under different dosages of UV or NIR irradiation (Figure 3b and Supplemental Figure 10). Under UV irradiation, the cell viability decreased significantly with time, and most cells were dead after 15 min of UV irradiation. These results are consistent with the observations from other groups and our previous observations[61,62]. In contrast, no significant photocytotoxicity was detected from NIR irradiation with the dosages used for the decaging experiments in this work. These data indicate that our DNAzyme-UCNP and NIR light have minimal toxic effects on cells.

To investigate if the DNAzyme-UCNP probe can be delivered into cells without any transfection agent and then used to image intracellular Zn^{2+}, we first incubated the conjugated sensor with HeLa cells overnight and used two-photon confocal microscopy to image the UCNP localization intracellularly. As shown in Figure 3c, we observed minimal intracellular luminescence emission in the absence of UCNP and clear luminescence from UCNPs in the presence of UCNP alone and DNAzyme-UCNP, indicating efficient cellular transfection. We then used confocal microscopy to monitor the Zn^{2+} cellular distribution after NIR irradiation (Figure 3d, e, Supplemental Figure 11–16). Clear enhancement of fluorescence signals was observed after NIR irradiation compared with the pre-irradiation. To eliminate non-specific cleavage or substrate dehybridization as an artifact, we repeated the experiment using a substrate strand that has the same construct except the critical ribonucleotide adenine was mutated into the deoxyribonucleo-tide form, deoxyadenosine, to render the substrate non-cleavable in the presence of Zn^{2+}. Minimal enhancement was observed after NIR irradiation. Together these data indicate that 1) the DNAzyme sensor has been delivered into the cytoplasm by the UCNP, 2) the substrate strand has been photo-decaged after NIR irradiation, and 3) the elevation of the fluorescence signal reflects the cleavage of substrate strands by low concentration intracellular Zn^{2+}.

To further confirm that this intracellular fluorescence increase is due to the presence of Zn^{2+}, we applied a high Zn^{2+} concentration in the culture medium and the Zn^{2+}-specific ionophore, pyrithione, to transport Zn^{2+} into the cytoplasm (Figure 3d, e, Supplemental Figure 11–16). By pyrithione, the intra-cellular Zn^{2+} concentration can be enriched to be equal to the extracellular Zn^{2+} concentration in the culture medium.[63,64] A further increase of fluorescent signal was observed, indicating the ability of the sensor to test ectopic

enrichment of Zn^{2+} in HeLa cells, and further confirming the proper function of this sensor in living cells.

To demonstrate the utility of our DNAzyme-UCNP sensor for imaging Zn^{2+} *in vivo*, we performed microinjection to deliver the sensor into zebrafish embryos, and to record Zn^{2+} distribution patterns using confocal microscopy. First, we assessed embryonic viability after the microinjection. As shown in Figure 4a, in contrast to almost complete loss of the viability within one day in the negative viability control, injecting DNAzyme-UCNP has a similar effect as no injection or injecting a saline solution (blank injection). More importantly, while UV irradiation resulted in gradual decrease in the viability over five days, NIR irradiation has a similar effect as no injection (Figure 4b), indicating that NIR is a safer and more reliable method for in *vivo* photo-controlled studies. As shown in Figure 4c and Supplemental Figure 17 and 18, a clear enhancement of fluorescence signals was observed inside zebrafish embryos after NIR irradiation compared with that before the NIR irradiation. As with the previous control using a non-cleavable substrate for cellular studies (see Figure 4c and Supplemental Figure 17 and 18), the same uncleavable construct did not show fluorescent enhancement, eliminating any artifact due to non-specific cleavage or spontaneous substrate dehybridization.

To demonstrate the *in vivo* imaging ability of the DNAzyme-UCNP sensor for metal ions beyond the early embryo stage, Zn^{2+} detection using this construct was also achieved in the more developed stage 3 days post-fertilization (3 dpf) of the fish larvae (Figure 5 and Supplemental Figure 19–21). Similar to the data from early stage embryos, a specific fluorescence signal was observed only from the active substrate constructs, but not from non-cleavable inactive substrate. Therefore, we have demonstrated successful temporal optical control of substrate strands decaging by a UCNP-based strategy and imaging of endogenous Zn^{2+} in zebrafish.

In this work we demonstrated optical control of imaging metal ions in *vivo* using DNAzyme-UCNPs sensor by exploiting optical upconversion. The novel photo-controllable Zn^{2+} nanosensor has been successfully designed and developed for the monitoring of Zn^{2+} distributions intracellularly and in vivo. This probe takes advantage of the efficient 365 nm light decaging in controllable the activity of the Zn^{2+}-specific DNAzyme and the ability of UCNP to generate 365 nm light from 980 nm NIR light in situ, as well as deep-tissue photon delivery ability of 980 nm NIR light. This design showcases two additional advantages for practical applications. First, UCNP conjugation serves as the delivery method of DNA based sensors into living cells through active endocytosis without any need of delivery agents required for many other sensors, including the majority of nucleic acid-based sensors. Second, the conjugation itself is a protective method to minimize DNA degradation because the nucleases' accessibility to the DNA based sensor will be blocked by the UCNP.[44,65]

Given the growing knowledge in Zn^{2+}-related diseases, especially in cancer research, increasingly research interests are focusing on Zn^{2+} detections in healthy and diseased models. As a leading vertebrate model organism in developmental biology and drug screening, zebrafish have been shown to be an excellent system in developing and demonstrating metal ion sensing and imaging agents, but methods to provide metal ions with

both spatial and time resolution are limited. The results presented in this work is consistent with those studies using fixed or sectioned zebrafish embryos and early stage larvae samples but provides additional time control in living zebrafish. For example, similar to those reported by Böhme *et al.* that used fixed zebrafish using laser ablation ICP-MS,[7] the result shown in Figure 4 and Supplemental Figures 17 and 18 showed consistently higher fluorescence signal from the embryonic cells than yolk region, indicating Zn^{2+} ion presents in both embryonic cells and egg yolk, but has higher concentration in embryonic cells. In later stage larvae, Bourassa *et al.* reported Zn^{2+} distribution is depleted from notochord structure but enriched in yolk by XRF tomography,[8] and independent research from Yan et al. using XRF[10] and Brun et al. using ICP-MS[9] depicted Zn^{2+} distribution in zebrafish head region. Compared with the published Zn^{2+} patterns in larvae stage, our data (Figure 5, Supplemental Figures 19–21) showed similar patterns, although we need to note that yolk tissue usually have strong autofluorescence and may not reflect accurate signal in our or others' studies.

Beside these observations published by other labs, we observed two new patterns by our Zn^{2+} DNAzyme-UCNP sensor. First, the fluorescence signal in 3 hpf embryos are more enriched in cells at the surface of the embryo, while depleted from cells adjacent to the yolk. This observation indicates that Zn^{2+} ion may have uneven distribution pattern as early as 3 hours during embryonic development and gives insight into tissue fate determination by Zn^{2+}-related proteins in future developmental biology research. Second, in 3 dpf fish larvae, we observed a group of multidendritic patterns along the zebrafish body and tail region, which are not reported by previous research. This absence of detailed Zn^{2+} pattern could be caused by the subtle structure break or signal loss during sample preparation procedures, which further emphasized the advantage of *in vivo* live imaging of metal ions. More detailed colocalization study could be performed in future research to characterize the new structure that have Zn^{2+} enrichment in fish larvae and to innovate the discovery of Zn^{2+} biofunctions in larvae stage.

Zn^{2+} is only one type of metal ions that proved to relate with specific diseases. As the mechanistic study of diseases dive into sub-cellular or even sub-molecular level, more roles of metal ions in in *vivo* biochemistry have been discovered, which lead to a growing demand for regulatable in *vivo* metal ion sensors with both spatial and time resolution. Since DNAzymes that are selective for many other metal ions already have been obtained, the method demonstrated in this work opens a new avenue for understanding the roles of not only Zn^{2+}, but generally to all other metal ions with selective DNAzymes.

EXPERIMENTAL SECTION

Instrumentation.

A JEOL 2100 Cryo transmission electron microscope with an accelerating voltage of 200kV was used to take all transmission electron microscopy (TEM) images of nanoparticles. FluoroMax-P fluorimeter (HORIBA Jobin Yvon Inc., Edison, NJ) modified with a commercial CW IR laser (ThorLabs, Inc., Edison, NJ) that emits 980 nm was used for fluorescent spectra measurements. Weight measurements were taken using an XS 105 Dual

range weighing balance. (Mettler Toledo., Chicago, IL). Software ImageJ was used to estimate the size of the nanoparticles.

Chemicals.

All chemicals were of analytical grade and were used without further purification. Rare earth acetates, Yttrium (III) acetate hydrate and Ytterbium (III)acetate hydrate with 99.9% trace metal basis were purchased from Sigma Aldrich. Erbium (III) acetate hydrate with 99.9% trace metal basis were purchased from Strem Chemicals. Oleic acid (90% technical grade), 1-Octadecene (90% technical grade), ammonium fluo-ride (≥ 99.99% trace metal basis), sodium hydroxide (semiconductor grade 99.99% trace metal basis), tetraethyl orthosilicate (≥ 99.0% G.C.), 3-mercaptopropyl trimethoxysilane (95%), 4-maleimidobutyric acid N-hydroxy-succinimide ester (≥ 98.0% HPLC), Polyvinylpyrrolidone were purchased from Sigma Aldrich. Ethanol was bought from Decon Laboratories Inc. while 10X Phosphate Buffered Saline was purchased from Lonza Inc. Ammonium hydroxide and Dimethyl sulfoxide (ACS Certified) and cyclohexane were purchased from Fisher Scientific.

DNA sequences.

DNA oligos are synthesized by the IDT company.

Particle conjugation: TTTTTTTTTTTTTTTTTTT-SH

FAM control: AAAAAAAAAAAAAAAAAAA-FAM

iS: FAM-ACT CAC TAT AGG AAG AGA TGG ACG TG-BHQ1

S: FAM-ACT CAC TAT Benz-rAGG AAG AGA TGG ACG TG-BHQ1

E: AAAAAAAAAAAAAAAAAAAACACGTCCATCTCTTCTCCGAGCCGGTCGAAATAG TGAGT-Dabcyl

iE: AAAAAAAAAAAAAAAAAAAACACGTCCATCTCTTCCCCGAGCCGGTCGAAATAG TGAGT-Dabcyl

Synthesis of Upconversion Nanoparticles (UCNP).

The synthesis procedure of upconversion nanoparticles (UCNP) was adopted from Wang et al.[66] with adequate modifications. In a 50-mL three-neck round-bottomed flask, 7 mL of 1-octadecene (ODE) and 3 mL of oleic acid (OA) was mixed with 2 mL of 0.2M $Ln(CH_3COO)_3$ (Ln = Y^{3+}, Yb^{3+}, Tm^{3+}) aqueous solution. The mixture was treated at 150 °C for 90 minutes to yield lanthanide oleate complexes in organic media. The bright yellow solution was cooled down to 50 °C. For core syntheses, a mixture of NaOH methanol solution (0.5 M, 2 mL) and NH4F methanol solution (0.4 M, 4 mL) were subsequently added. For core-shell syntheses and core-shell-shell syntheses, pre-made UCNP in cyclohexane was added to the reaction flask right before the addition of (NaOH-NH4F) mixture. After 30 minutes, the reaction mixture was brought to 100 °C for 15 minutes, and

then degassed for at least three times. The reaction mixture was then heated up to 300 °C for 2 hours under nitrogen. The final product was then washed for three times and re-dispersed in 4 mL of cyclohexane.

Calculation of Mass Concentration of Particles:

To each of the three pre-weighed glass vessels, 100 μL of nanocrystal colloids was added. The glass vessels were then placed in the oven for 30 minutes to evaporate the cyclohexane. Finally, the glass vessels containing dry nanocrystals were weighed again. The mass concentration of UCNP was calculated by dividing the difference in masses with 100 μL and taking the average. A 6-μL aliquot of nanocrystal colloids in cyclohexane was deposited onto a copper TEM grid coated with carbon, and the TEM grid was air-dried at room temperature, before imaging the nano-crystals using TEM. The average volume of nanocrystal was measured from the TEM image, so the average mass of each nanocrystal was obtained by multiplying the average volume by the density of NaYF4. The molar concentration could finally be determined by dividing the mass concentration by the average mass of each nanocrystal.

Silica Coating of UCNP.

The silica coating procedure was adopted from Graf et al. In a 1.5-mL plastic, 1 mL of the 4 mL stock solution of OA-capped UCNP dispersed in cyclohexane was mixed with 0.5 mL of ethanol and centrifuged at 15000 rpm for 25 minutes; after removing the supernatant, the resulting yellow pellet was re-suspended in 0.5 mL of ethanol via sonication. The 0.5 mL particle colloids in ethanol were mixed with 1 mL of 2 M HCl aqueous solution. The resultant solution was washed twice with 1 mL of ethanol, and twice with 1 mL of water via centrifugation at 15000 rpm for 25 minutes Finally, the ligand-free UCNP was re-dispersed in 1 mL of water. Next, in a 50-mL round-bottomed flask, 200 mg of PVP-k30 was mixed with 1 mL of UCNP colloids in water and 4 mL of water; the mixture was stirred for 2 hours and sonicated for 30 minutes before the addition of ethanol (20 mL). The resultant mixture was sonicated for 30 minutes before concentrated ammonia solution (1 mL) was added while stirring. The mixture was then sonicated for 30 minutes before the addition of 35 μL of tetraethyl orthosilicate (TEOS) under vigorous stirring overnight. The reaction proceeded at room temperature overnight (12 hours). Finally, the silica coated nanoparticles were washed 3 times with centrifugation at 15000 rpm for 25 minutes and re-suspended in 10 mL of ethanol

Amine Modification of Silica-coated UCNP (SiO_2@UCNP).

First, 4 mL of SiO2@UCNP was mixed with 6 mL of ethanol in a 50-mL round-bottomed flask. The flask was sealed with para-film and sonicated for 30 minutes. After that, 600 μL of (3-Aminopropyl) trimethoxysilane (APTMS) was added to the flask under stirring. The flask was allowed to reflux in an oil bath at 110 °C for 24 hours. After 24 hours of reaction, the mixture and the ethanol rinse of the flask was transferred to 8 1.5-mL microtubes; the solution was centrifuged at 15000 rpm for 25 minutes for three times before resuspension in 1 mL of ethanol via sonication.

Sulfo-SMCC conjugation of amine-modified UCNP (NH2@SiO_2@UCNP).

The NH2@SiO_2@UCNP colloidal solution in the 4 tubes from previous modification was centrifuged at 15000 rpm for 25 minutes; once removed the supernatant, pellet in each tube was re-dispersed in 1 mL of 1× HEPES buffer. This washing process was repeated three times. During the final wash, NH2@SiO_2@UCNP particles in each tube was re-dispersed in 700 μL of 1× HEPES buffer, before mixing with sulfo-SMCC solution (1 mg in 300 μL DMF). The mixture in the four tubes was mixed for six hours to afford the maleimide-activated UCNP. The maleimide-activated UCNP was centrifuged at 15000 rpm for 25 minutes and re-dispersed in 1 mL of 1x PBS buffer. This washing process was repeated three times. During the final wash, maleimide-activated UCNP in each tube was re-dispersed in 700 μL of 1× PBS buffer.

ssDNA functionalization of maleimide-activated UCNP.

About 7 mg of tris(2-carboxyethyl)phosphine hydrochloride salt (TCEP) was dissolved in 250 μL of Tris-acetate buffer (pH =5.25) to afford a freshly-prepared 0.1 M TCEP stock solution. In each of the four tubes, 60 μL of TCEP solution was mixed with 20 nmol of thiolated ssDNA, and Tris-acetate buffer (pH=5.25) was added to top up the total volume to 320 μL. The mixture in the four tubes was allowed to react for one hour, to afford reduced thiolated ssDNA. The solution was then transferred to the top part of a 3k Amicon tube. After centrifuging at 13200 rpm for 17 min, 300 μL of DI H2O was added to the top phase of the 3k Amicon tube, while the bottom phase was discarded. This washing process was repeated three times. During the final wash, the top phase (20~40 μL) was added to the freshly washed maleimide-activated UCNP solution. The mixture was mixed for 24 hours before centrifuging at 15000 rpm for 25 minutes and re-dispersed in 1 mL of 1× PBS. This washing process was repeated three times, during which the supernatants were discarded. DNA-functionalized UCNP in each tube was finally re-suspended in 1 mL of 1× PBS. The average number of OligoT20 DNA conjugated on each UCNP is 128. The ssDNA-functionalized UCNP (T20@UCNP) was stored at 4 °C

DNAzyme adsorption onto ssDNA-functionalized UCNP (T20@UCNP).

To avoid DNAzyme degradation, the solvent of T20@UCNP was switched from 1× PBS to 1× chelex-extracted Tris treated with Chelex-100 beads (pH=7.42). The particles were centrifuged at 15000 rpm for 25 minutes; after removal of the supernatant, the pellet was re-suspended in 1 mL of Tris buffer pre-treated with Chelex-100. This procedure was repeated three times to remove any metal ions that could cause DNAzyme degradation. In a 1.5-mL microtube, 1.0 μL of enzyme strand with an A20 tail, 1.0 μL of substrate strand and 18.0 μL of 1× Chelex-treated Tris buffer were mixed. The DNAzyme was annealed at 95 °C for 5 minutes and cooled in ice for 15 minutes, before the addition of T20@UCNP (20 μL in 1× Chelex-treated Tris buffer). The mixture of DNAzyme and UCNP was vortexed and then cooled in ice for another 15 minutes. After repeating this procedure three times, the particles were washed three times: During each time, the particles were centrifuged at 3000 rpm for 1 minutes; once removed the supernatant, the pellet was re-suspended in 40.0 μL of 1× Chelex-treated Tris buffer; sonication was used to re-disperse the DNAzyme-adsorbed UCNP only during the final wash. The average number of DNAzyme sensor molecules

hybridized on each UCNP is 31. The DNAzyme-adsorbed UCNP would be ready for activity assay by the end of the wash.

Cell Culture and Sensor Delivery Study:

HeLa cells were cultured in Dulbecco's modification of Eagle's medium (DMEM) supplemented with 10% Fetal Bovine Serum (FBS), 100 U/mL penicillin, and 100 U/mL streptomycin, on 25 cm2 culture flasks at 37 degrees C in a humidified 5% CO2 incubator. Before imaging, cells were plated in 35 mm glass-bottom dishes (MatTek) and grown to 50–70% confluence.

The DNAzyme-UCNP sensor is directly added into the cell culture petridish for nanoparticle-based transfection. The stock DNAzyme-UCNP concentration is estimated to be 2 nM final concentration. After overnight transfection, cells were washed thoroughly with PBS to remove excess amount of DNAzyme-UCNP in the medium. Specific organelles inside cells were stained with commercial dyes, such as Hoechst 33258 and LysoTracker Red DND-99. Images were obtained using a Zeiss LSM 710 NLO confocal microscope at 20x magnification equipped with a Mai-Tai Ti-Sapphire laser. Luminescence emission of UCNPs was obtained by exciting at 980 nm and measuring over 450–617 nm. The pinhole and gain settings were kept constant throughout the whole imaging process.

Intracellular Zinc Sensing:

After transfection and washing steps with DPBS, HeLa cells were immersed in 200 μl DMEM and irradiated by NIR laser light (~ 1W/cm^2) at 980 nm for 15 minutes. Immediately after NIR treatment, cells were imaged for the post-NIR group. Fluorescent images were taken again after 15 minutes incubation, allowing reaction of activated DNAzyme sensor under endogenous Zn^{2+} concentration intracellularly. Stock solutions of zinc ionophore pyrithione (PT) with $ZnCl_2$ were added to the cells at final concentrations of 100 μM. Another 30 minutes incubation was given to allow exogenous Zn^{2+} delivery into cells and trigger the reaction of the activated DNAzyme sensor. Fluorescent images were taken immediately after incubation.

Images were obtained using a Zeiss LSM 710 NLO confocal microscope at 20x magnification. Fluorescence emission of Hoechst 33258 was measured over 415–475 nm ranges, with excitation at 401 nm. Fluorescence emission of LysoTracker was obtained by exciting at 561 nm and measuring over 570–735 nm. Fluorescence emission of FAM was obtained by exciting at 488 nm and measuring over 497–550 nm. The pinhole and gain settings were kept constant throughout the whole imaging process.

Zebrafish Housing.

A total of 20 adult (4 to 7 months) wild-type AB strain zebrafish (~ 50:50 male:female ratio) were obtained from the Zebrafish International Resource Center. All fish were housed in groups of ~ 10 per 10 L tank. Adult zebrafish were maintained in a Z-hab mini system (Aquatic habitats, Beverly, MA) fish facility at 28.5 °C on a 14h:10h light:dark cycle according to standard protocols. Fish were fed Tetramin Tropical Flakes (Tetra USA, Blacksburg, VA) twice daily. Following observation, animals were euthanized with 500

mg/L Tricaine and held on ice. All experimental procedures were carried out in compliance with National and Institutional guidelines on animal experimentation and care. The spawning of eggs was triggered by giving light stimulation. Zebrafish embryos were maintained in E3 embryo media.

Fish Embryo Injection and Imaging.

Unlike neutral small molecules, the UCNP size and negative charge from DNAzyme sensors will not allow direct delivery of this sensor into zebrafish embryos or larvae by directly soaking. This is especially true for early stage zebrafish embryos, since there is an outer chorion envelope surrounding the zebrafish embryo protecting the inner embryo from the outer environment. Therefore, to study metal ion distributions in early stage model organisms, microinjection is the most reliable and quantitative method to guarantee efficient and accurate sensor delivery.

The influences of microinjection operation, UCNP sensor toxicity, NIR phototoxicity were assessed, and have been proved to be minimal by phenotypical studies up to five days of zebrafish embryonic development. After embryo collection, embryos were injected at the single-cell stage with the injection platform. Embryos were handled under yellow light to avoid early decaging and unwanted activation. ~ 5 pl of sample was injected into each embryo with ~ 20 nM DNAzyme-UCNP sensor. Alternatively, inactive substrate and enzyme strands combinations were used as controls. Control injections using embryo media was performed to assess the influence of the injection technique to the zebrafish development. To avoid early degradation and unwanted activation of the DNAzyme-UCNP sensor during injection steps, all the injection procedures were performed under yellow light.

Microinjector needles, borosilicate glass capillaries (1B100F-4, World Precision Instruments), were prepared in advance using a micropipette puller (P-2000, Sutter Instrument Company) and with a final capillary opening of approximately 10 μm. While the microinjection solution was incubating, fish were allowed to spawn by removing a divider separating male and female zebrafish in the tanks. Fertilized eggs were collected immediately after spawning, approximately 20 min later, and collected with a tea strainer in room temperature 0.3x Danieau’s solution. Single embryos were transferred and aligned against a microscope slide in a Petri dish using a Pasteur pipette. The microinjection needle was backfilled with 3 μl of microinjection solution and injected into the cytoplasm of one-cell stage embryos using a pressure injector (IM-300, Narishige). The total injection volume was approximately 3–4 nanoliter per embryo. Embryos were allowed to develop for 48 hours in 0.3x Danieau’s solution prior to screening for transgene expression and selection for experiments.

The injected zebrafish embryos were imaged directly after injection or cultured until 3 dpf larvae. Similar 980 nm NIR irradiation steps were performed before confocal imaging. Images were obtained using a Zeiss LSM 710 NLO and a Zeiss LSM 880 confocal microscope at 5x and 10x magnification. Fluorescence emission of FAM in zebrafish embryos and larvae was obtained by exciting at 488 nm and measuring over 492–707 nm and 497–549 nm respectively. The pinhole and gain settings were kept constant throughout the whole imaging process.

Supplementary Material

Refer to Web version on PubMed Central for supplementary material.

ACKNOWLEDGMENTS

We wish to thank the U.S. National Institutes of Health (GM124316 and MH110975) for financial support, Dr. Yuting Wu and Mingkuan Lyu for assisting with fish NIR irradiation and imaging, Yiming Wang for helping with TEM measurements, Dr. Kai Zhang, Dr. Yuting Wu, Ryan Lake, Greg Pawel, Dr. Jingjing Zhang, Dr. Claire McGhee, for helpful discussions and comments.

REFERENCES

(1). Dalmark M The effect of ionic strength on cell volume, cell pH and cellular buffer capacity in human red blood cells, 1981; Vol. 40.

(2). Quartin RS; Wetmur JG Effect of ionic strength on the hybridization of oligodeoxynucleotides with reduced charge due to methylphosphonate linkages to unmodified oligodeoxynucleotides containing the complementary sequence. Biochemistry 1989, 28, 1040. [PubMed: 2713356]

(3). Fondacaro J Intestinal ion transport and diarrheal disease. Am. J. Physiol. Gastrointest. Liver Physiol. 1986, 250, G1.

(4). Kozlowski H; Janicka-Klos A; Brasun J; Gaggelli E; Valensin D; Valensin G Copper, iron, and zinc ions homeostasis and their role in neurodegenerative disorders (metal uptake, transport, distribution and regulation). Coord. Chem. Rev 2009, 253, 2665.

(5). Boynton AL; McKeehan WL; Whitfield JF Ions, cell proliferation, and cancer; Academic Press, 2013.

(6). Gaeta A; Hider RC The crucial role of metal ions in neurodegeneration: the basis for a promising therapeutic strategy. Br. J. Pharmacol 2005, 146, 1041. [PubMed: 16205720]

(7). Böhme S; Baccaro M; Schmidt M; Potthoff A; Stärk H-J; Reemtsma T; Kühnel D Metal uptake and distribution in the zebrafish (Danio rerio) embryo: differences between nanoparticles and metal ions. Environ. Sci. Nano 2017, 4, 1005.

(8). Bourassa D; Gleber S-C; Vogt S; Yi H; Will F; Richter H; Shin CH; Fahrni CJ 3D imaging of transition metals in the zebrafish embryo by X-ray fluorescence microtomography. Metallomics 2014, 6, 1648. [PubMed: 24992831]

(9). Brun NR; Lenz M; Wehrli B; Fent K Comparative effects of zinc oxide nanoparticles and dissolved zinc on zebrafish embryos and eleuthero-embryos: Importance of zinc ions. Sci. Total Environ. 2014, 476–477, 657.

(10). Yan G; Zhang Y; Yu J; Yu Y; Zhang F; Zhang Z; Wu A; Yan X; Zhou Y; Wang F Slc39a7/zip7 Plays a Critical Role in Development and Zinc Homeostasis in Zebrafish. PLoS ONE 2012, 7, e42939. [PubMed: 22912764]

(11). Xu H; Li Q; Wang L; He Y; Shi J; Tang B; Fan C Nanoscale optical probes for cellular imaging. Chem. Soc. Rev 2014, 43, 2650. [PubMed: 24394966]

(12). Shao Q; Xing B Photoactive molecules for applications in molecular imaging and cell biology. Chem. Soc. Rev 2010, 39, 2835. [PubMed: 20480074]

(13). Chen S; Weitemier AZ; Zeng X; He L; Wang X; Tao Y; Huang AJ; Hashimotodani Y; Kano M; Iwasaki H Near-infrared deep brain stimulation via upconversion nanoparticle-mediated optogenetics. Science 2018, 359, 679. [PubMed: 29439241]

(14). Carter KP; Young AM; Palmer AE Fluorescent Sensors for Measuring Metal Ions in Living Systems. Chem. Rev 2014, 114, 4564. [PubMed: 24588137]

(15). Zeng L; Miller EW; Pralle A; Isacoff EY; Chang CJ A Selective Turn-On Fluorescent Sensor for Imaging Copper in Living Cells. J. Am. Chem. Soc 2006, 128, 10. [PubMed: 16390096]

(16). Chyan W; Zhang DY; Lippard SJ; Radford RJ Reaction-based fluorescent sensor for investigating mobile Zn2+ in mitochondria of healthy versus cancerous prostate cells. Proc. Natl. Acad. Sci. U. S. A 2014, 111, 143. [PubMed: 24335702]

(17). Fahrni CJ; O'Halloran TV Aqueous Coordination Chemistry of Quinoline-Based Fluorescence Probes for the Biological Chemistry of Zinc. J. Am. Chem. Soc 1999, 121, 11448.

(18). Zhang J; Cheng F; Li J; Zhu J-J; Lu Y Fluorescent nanoprobes for sensing and imaging of metal ions: Recent advances and future perspectives. Nano today 2016, 11, 309. [PubMed: 27818705]

(19). Xing H, University of Illinois at Urbana-Champaign, 2015.

(20). Wu P; Hwang K; Lan T; Lu Y A DNAzyme-gold nanoparticle probe for uranyl ion in living cells. J. Am. Chem. Soc 2013, 135, 5254. [PubMed: 23531046]

(21). Xing H; Wong NY; Xiang Y; Lu Y DNA aptamer functionalized nanomaterials for intracellular analysis, cancer cell imaging and drug delivery. Curr. Opin. Chem. Biol 2012, 16, 429. [PubMed: 22541663]

(22). Hirayama T; Van de Bittner GC; Gray LW; Lutsenko S; Chang CJ Near-infrared fluorescent sensor for in vivo copper imaging in a murine Wilson disease model. Proc. Natl. Acad. Sci. U. S. A 2012, 109, 2228. [PubMed: 22308360]

(23). Zhang J; Smaga LP; Satyavolu NSR; Chan J; Lu Y DNA aptamer-based activatable probes for photoacoustic imaging in living mice. J. Am. Chem. Soc 2017, 139, 17225. [PubMed: 29028325]

(24). Breaker RR; Joyce GF A DNA enzyme that cleaves RNA. Chem. Biol 1994, 1, 223. [PubMed: 9383394]

(25). Liu Y; Sen D Local Rather than Global Folding Enables the Lead-dependent Activity of the 8–17 Deoxyribozyme: Evidence from Contact Photo-crosslinking. J. Mol. Biol 2010, 395, 234. [PubMed: 19917290]

(26). Sekhon GS; Sen D A Stereochemical Glimpse of the Active Site of the 8–17 Deoxyribozyme from Iodine-Mediated Cross-Links Formed with the Substrate's Scissile Site. Biochemistry 2010, 49, 9072. [PubMed: 20839874]

(27). Lan T; Lu Y In Interplay between Metal Ions and Nucleic Acids; Springer: 2012, p 217.

(28). Zhang X-B; Kong R-M; Lu Y Metal ion sensors based on DNAzymes and related DNA molecules. Annu. Rev. Anal. Chem 2011, 4, 105.

(29). Liu J; Cao Z; Lu Y Functional nucleic acid sensors. Chem. Rev 2009, 109, 1948. [PubMed: 19301873]

(30). Li Y; Lu Y; New York: Springer: 2009.

(31). Tuerk C; Gold L Systematic evolution of ligands by exponential enrichment: RNA ligands to bacteriophage T4 DNA polymerase. Science 1990, 249, 505. [PubMed: 2200121]

(32). Ellington AD; Szostak JW In vitro selection of RNA molecules that bind specific ligands. Nature 1990, 346, 818. [PubMed: 1697402]

(33). Li Y A quarter century of in vitro selection. J. Mol. Evol 2015, 81, 137. [PubMed: 26597944]

(34). Santoro SW; Joyce GF A general purpose RNA-cleaving DNA enzyme. Proc. Natl. Acad. Sci. U. S. A 1997, 94, 4262. [PubMed: 9113977]

(35). Breaker RR; Joyce GF A DNA enzyme with Mg2+-dependent RNA phosphoesterase activity. Chem. Biol 1995, 2, 655. [PubMed: 9383471]

(36). Li J; Zheng W; Kwon AH; Lu Y In vitro selection and characterization of a highly efficient Zn (II)-dependent RNA-cleaving deoxyribozyme. Nucleic Acids Res. 2000, 28, 481. [PubMed: 10606646]

(37). Liu J; Brown AK; Meng X; Cropek DM; Istok JD; Watson DB; Lu Y A catalytic beacon sensor for uranium with parts-per-trillion sensitivity and millionfold selectivity. Proc. Natl. Acad. Sci. U. S. A 2007, 104, 2056. [PubMed: 17284609]

(38). Torabi S-F; Wu P; McGhee CE; Chen L; Hwang K; Zheng N; Cheng J; Lu Y In vitro selection of a sodium-specific DNAzyme and its application in intracellular sensing. Proc. Natl. Acad. Sci. U. S. A 2015, 201420361.

(39). Zhou W; Saran R; Huang PJJ; Ding J; Liu J An exceptionally selective DNA cooperatively binding two Ca2+ ions. ChemBioChem 2017, 18, 518. [PubMed: 28087991]

(40). Saran R; Liu J A silver DNAzyme. Anal. Chem 2016, 88, 4014. [PubMed: 26977895]

(41). Zhou W; Vazin M; Yu T; Ding J; Liu J In Vitro Selection of Chromium-Dependent DNAzymes for Sensing Chromium (III) and Chromium (VI). Chem.–Eur. J 2016, 22, 9835. [PubMed: 27249536]

(42). Huang P-JJ; Liu J Rational evolution of Cd2+-specific DNAzymes with phosphorothioate modified cleavage junction and Cd2+ sensing. Nucleic Acids Res. 2015, 43, 6125. [PubMed: 25990730]

(43). Lan T; Furuya K; Lu Y A highly selective lead sensor based on a classic lead DNAzyme. Chem. Commun 2010, 46, 3896.

(44). McGhee CE; Loh KY; Lu Y DNAzyme sensors for detection of metal ions in the environment and imaging them in living cells. Curr. Opin. Biotechnol 2017, 45, 191. [PubMed: 28458112]

(45). Xiang Y; Lu Y DNA as sensors and imaging agents for metal ions. Inorg. Chem 2013, 53, 1925. [PubMed: 24359450]

(46). Torabi S-F; Lu Y Functional DNA nanomaterials for sensing and imaging in living cells. Curr. Opin. Biotechnol 2014, 28, 88. [PubMed: 24468446]

(47). Chaulk SG; MacMillan AM Caged RNA: photo-control of a ribozyme reaction. Nucleic Acids Res. 1998, 26, 3173. [PubMed: 9628915]

(48). Chaulk SG; MacMillan AM Synthesis of oligo-RNAs with photocaged adenosine 2'-hydroxyls. Nat. Protoc 2007, 2, 1052. [PubMed: 17546010]

(49). Hwang K; Wu P; Kim T; Lei L; Tian S; Wang Y; Lu Y Photocaged DNAzymes as a general method for sensing metal ions in living cells. Angew. Chem. Int. Ed 2014, 53, 13798.

(50). Wu Z; Fan H; Satyavolu NSR; Wang W; Lake R; Jiang JH; Lu Y Imaging Endogenous Metal Ions in Living Cells Using a DNAzyme–Catalytic Hairpin Assembly Probe. Angew. Chem. Int. Ed 2017, 56, 8721.

(51). Yang Y; Shao Q; Deng R; Wang C; Teng X; Cheng K; Cheng Z; Huang L; Liu Z; Liu X In vitro and in vivo uncaging and bioluminescence imaging by using photocaged upconversion nanoparticles. Angew. Chem 2012, 124, 3179.

(52). Li L-L; Wu P; Hwang K; Lu Y An exceptionally simple strategy for DNA-functionalized up-conversion nanoparticles as biocompatible agents for nanoassembly, DNA delivery, and imaging. J. Am. Chem. Soc 2013, 135, 2411. [PubMed: 23356394]

(53). Li L; Lu Y In DNA Nanotechnology; Springer: 2013, p 277.

(54). Li LL; Zhang R; Yin L; Zheng K; Qin W; Selvin PR; Lu Y Biomimetic surface engineering of lanthanide-doped upconversion nanoparticles as versatile bioprobes. Angew. Chem 2012, 124, 6225.

(55). Wang F; Banerjee D; Liu Y; Chen X; Liu X Upconversion nanoparticles in biological labeling, imaging, and therapy. Analyst 2010, 135, 1839. [PubMed: 20485777]

(56). Peng J; Xu W; Teoh CL; Han S; Kim B; Samanta A; Er JC; Wang L; Yuan L; Liu X High-efficiency in vitro and in vivo detection of Zn2+ by dye-assembled upconversion nanoparticles. J. Am. Chem. Soc 2015, 137, 2336. [PubMed: 25626163]

(57). Wang F; Liu X Upconversion multicolor fine-tuning: visible to near-infrared emission from lanthanide-doped NaYF4 nanoparticles. J. Am. Chem. Soc 2008, 130, 5642. [PubMed: 18393419]

(58). Li Z; Zhang Y Monodisperse Silica-Coated Polyvinylpyrrolidone/NaYF4 Nanocrystals with Multicolor Upconversion Fluorescence Emission. Angew. Chem. Int. Ed 2006, 45, 7732.

(59). Li L-L; Yin Q; Cheng J; Lu Y Polyvalent Mesoporous Silica Nanoparticle-Aptamer Bioconjugates Target Breast Cancer Cells. Adv. Healthcare Mater. 2012, 1, 567.

(60). Wang W; Satyavolu NSR; Wu Z; Zhang JR; Zhu JJ; Lu Y Near-Infrared Photothermally Activated DNAzyme-Gold Nanoshells for Imaging Metal Ions in Living Cells. Angew. Chem. Int. Ed 2017, 56, 6798.

(61). Stoien JD; Wang RJ Effect of Near-Ultraviolet and Visible Light on Mammalian Cells in Culture II. Formation of Toxic Photoproducts in Tissue Culture Medium by Blacklight. Proc. Natl. Acad. Sci. U. S. A 1974, 71, 3961. [PubMed: 4530275]

(62). Meechan PJ; Wilson C Use of Ultraviolet Lights in Biological Safety Cabinets: A Contrarian View. Appl. Biosaf 2006, 11, 222.

(63). Huang Z; Lippard SJ In Methods Enzymol.; Conn PM, Ed.; Academic Press: 2012; Vol. 505, p 445. [PubMed: 22289467]

(64). Buccella D; Horowitz JA; Lippard SJ Understanding zinc quantification with existing and advanced ditopic fluorescent Zinpyr sensors. J. Am. Chem. Soc 2011, 133, 4101. [PubMed: 21351756]

(65). Rosi NL; Giljohann DA; Thaxton CS; Lytton-Jean AK; Han MS; Mirkin CA Oligonucleotide-modified gold nanoparticles for intracellular gene regulation. Science 2006, 312, 1027. [PubMed: 16709779]

(66). Wang F; Han Y; Lim CS; Lu Y; Wang J; Xu J; Chen H; Zhang C; Hong M; Liu X Simultaneous phase and size control of upconversion nanocrystals through lanthanide doping. Nature 2010, 463, 1061. [PubMed: 20182508]

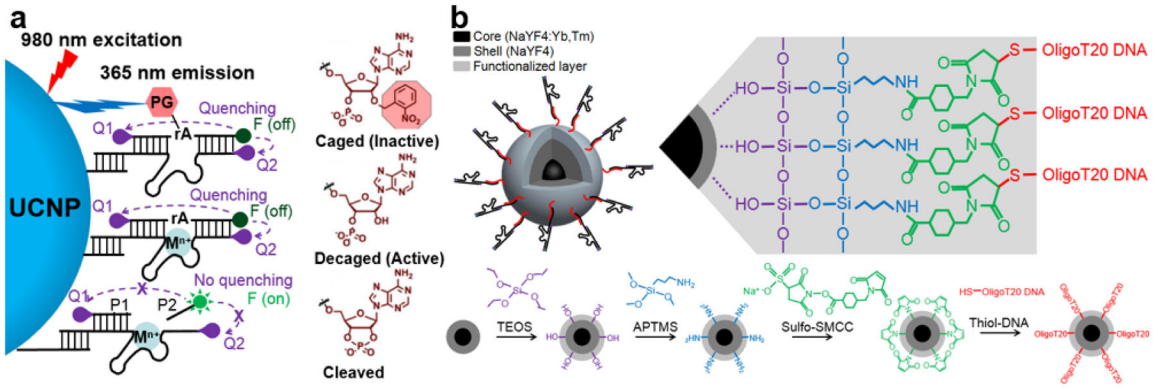

Figure 1:

Schematic illustration showing the synthesis of photo controllable UCNP and DNAzyme-based nanosensor and its response to Zn^{2+}. (a) Schematics of NIR metal ion sensor. A fluorophore (F) and a quencher (Q1) are functionalized to opposite ends of the substrate strand, with another quencher (Q2) on the enzyme strand. A 2'-nitrobenzyl photocage group (PG) is added to protect the ribonucleotide adenosine (rA) site in the substrate strand from being cleaved, which is photo-dissociated under 365 nm emission from UCNP. After metal ion specific cleavage, the substrate strand is broken into two product strands (P1 and P2), and the P2 strand with fluorophore is dehybridized from the enzyme strand due to the reduced melting temperature, causing fluorescence turn-on. The structures of the riboadenosine at the cleaving site with the photocage modification, after decaging activation, and after cleavage are shown. (b) Schematics of DNA functionalization of UCNP. The core-shell UCNP were coated with silica using tetraethyl orthosilicate (TEOS) to generate hydroxyl groups at the surface. Then, (3-Aminopropyl)trimethoxysilane (APTMS) was used to functionalize the particles with amine groups, and Sulfo-SMCC was applied to functionalize maleimide groups on the surface. Thiol-modified DNA was then conjugated to the maleimide groups to generate DNA functionalized UCNPs.

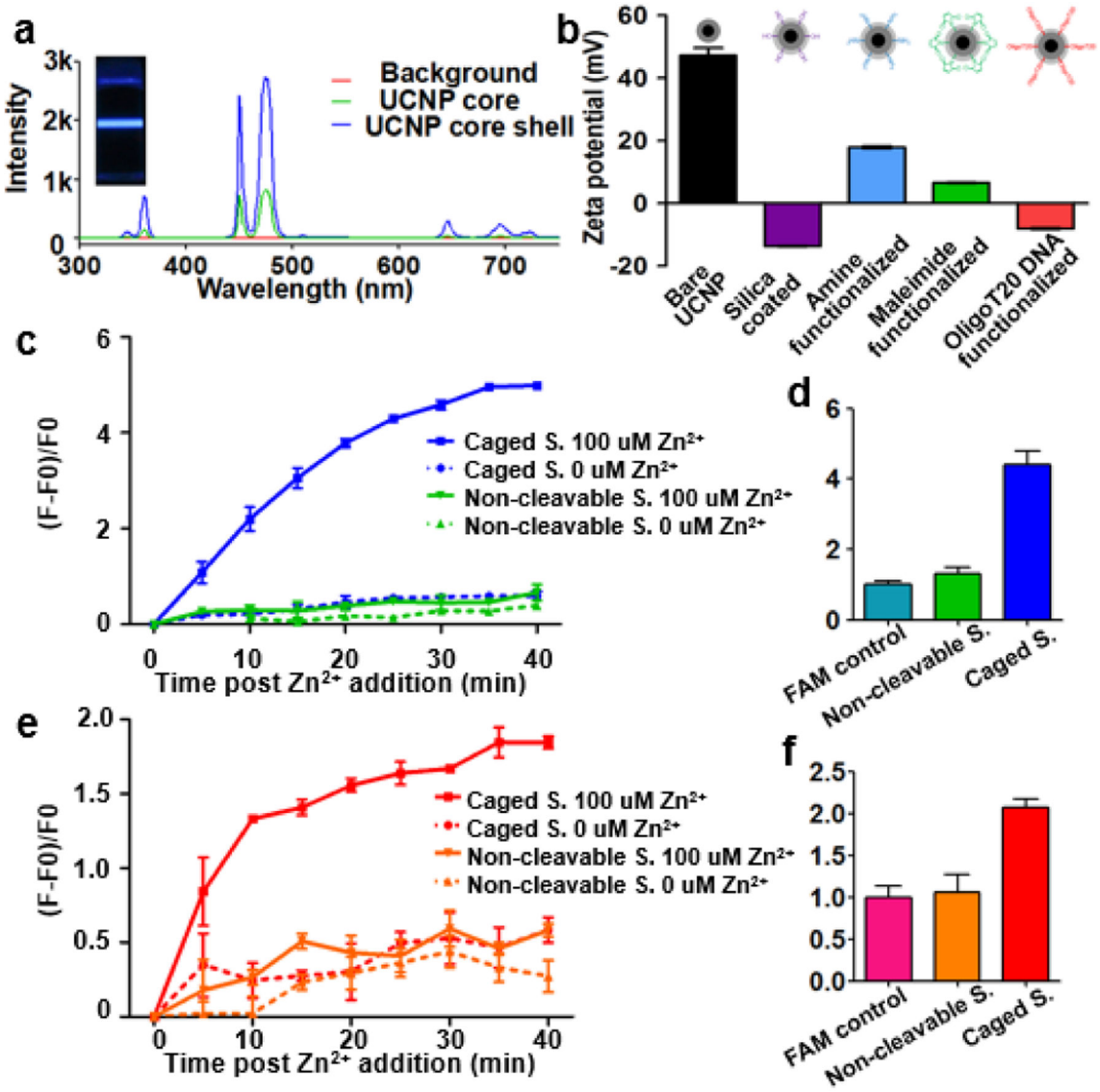

Figure 2.

In *vitro* characterization of the UCNP and DNAzyme-based Zn^{2+} nanosensor. (a) Upconversion luminescence spectra of the $NaYF_4$:Yb/Tm (49:1) core and $NaYF_4$:Yb/Tm(49:1) @$NaYF_4$ core shell UCNPs under the 980 nm excitation. Inserted photograph showing the color of UCNP under 980 nm irradiation. (b) Zeta potential pattern of UCNPs during step-by-step functionalization, showing that all the steps in functionalization are well-indexed. Before any functionalization, the bare UCNPs are positively charged. The silica layer has a negatively charged surface due to their hydroxyl groups. Amine and maleimide functionalities make the charge of the UCNP surface back to positive. Finally, the negatively-charge carrying DNA makes the general charge of functionalized UCNPs slightly negative. (c, d) Response of the DNAzyme-UCNP sensor after UV irradiation decaging by kinetic plot of 520 nm emission (c) and endpoint (75 min) emission (d). (e,f) Response of the DNAzyme-UCNP sensor after NIR irradiation decaging by kinetic plot of 520 nm emission (e) and endpoint (75 min) emission (f). Kinetics and endpoint graphs are from

three replicates and show mean and standard deviation. The “F” stands for the intensity of fluorescence signal from measurement during the experiment, and the “F0” stands for the intensity of background fluorescence at the start of the experiment in (c) and (e).

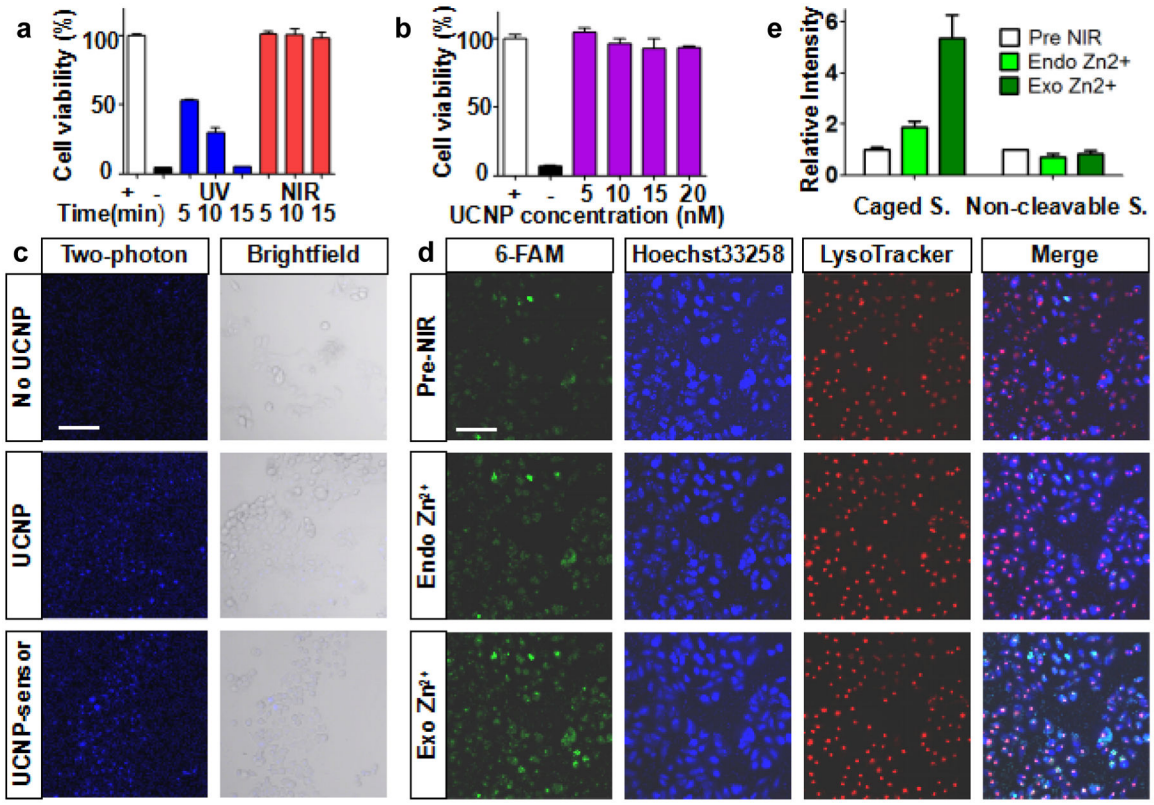

Figure 3:

Intracellular Zn^{2+} detection by UCNP and DNAzyme-based nanosensor. (a,b) Cytotoxicity of (a) NIR and UV exposure and (b) Zn^{2+} sensor. '+' for no treatment control group; '−' for 50 μM H_2O_2 treatment group, which shows strong toxicity to cells and is used as a toxicity control. Graph shows mean and standard deviation. (c) Luminescence emission of UCNP under 980 nm excitation by two-photon confocal imaging, showing intracellular delivery of the Zn^{2+} sensor. Clear increase of UCNP upconversion signal was detected from UCNP transfection groups compared with no UCNP groups. Scale bar: 50 μm. (d,e) Representative confocal images (d) and quantitative analysis (e) of intracellular Zn^{2+} detection by the Zn^{2+} sensor in HeLa cells, showing sensor turn-on (green channel) in response to endogenous and 100 μM exogenous Zn^{2+}. Cell nuclei and lysosomes were labeled by Hoechst 33258 (blue) and LysoTracker (red) respectively. Scale bar: 100 μm. Cytotoxicity and fluorescence intensity graphs are from three replicates and show mean and standard deviation.

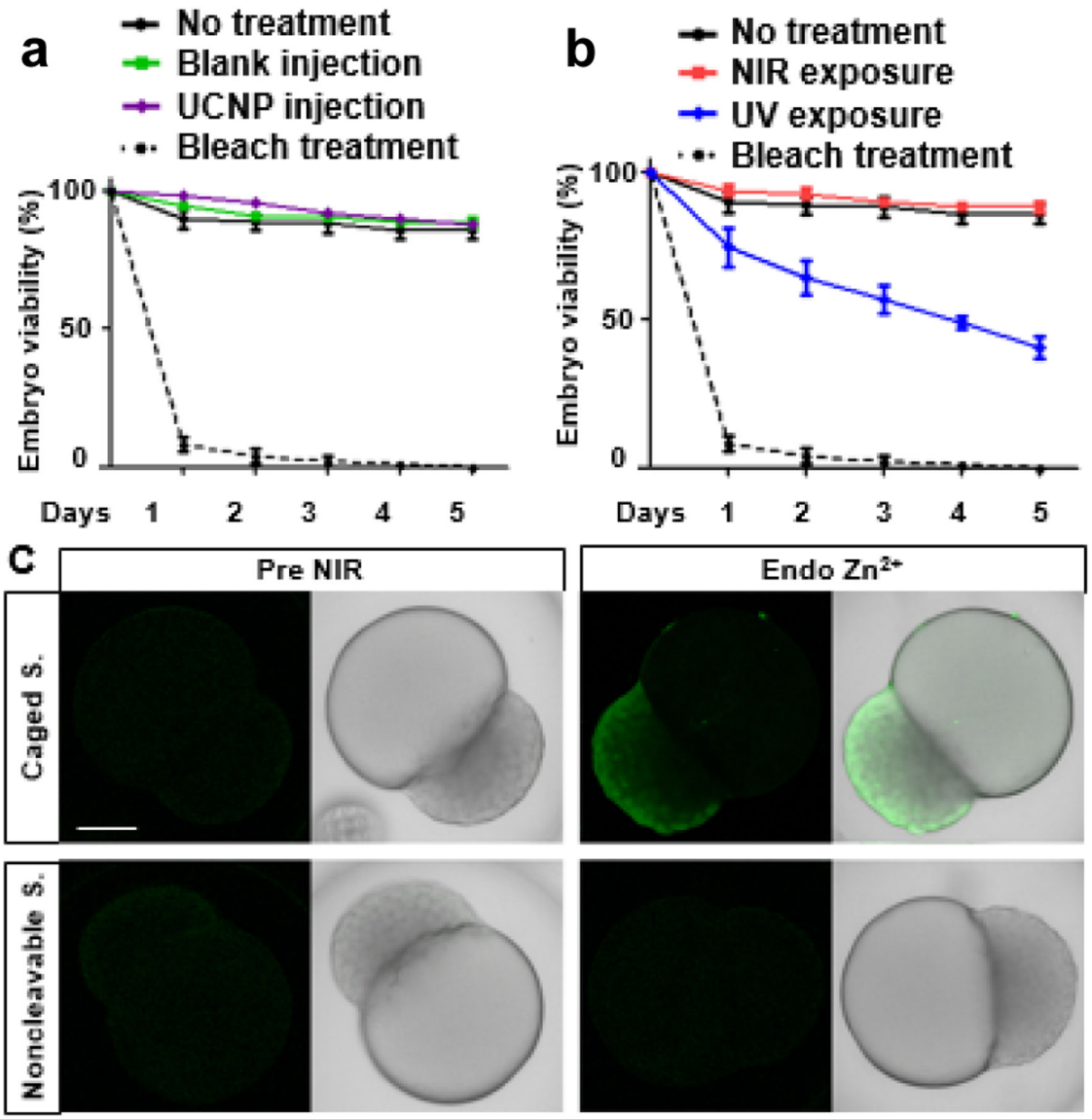

Figure 4:

In *vivo* Zn^{2+} detection in early embryos by NIR photoactivation sensor. (a,b) Embryonic toxicity of (a) Zn^{2+} sensor injection and (b) NIR exposure. (c) Representative confocal images of Zn^{2+} detection by the Zn^{2+} sensor in zebrafish embryos. Consistent with intracellular data, an increase of fluorescence signal in response to endogenous Zn^{2+} was observed. No signal increase was observed from control groups using a non-cleavable inactive substrate strand in the sensor. Scale bar: 200 μm. "Pre NIR" groups show the background fluorescence signal. "Endo Zn^{2+}" groups show the fluorescence generated under endogenous Zn^{2+} from NIR-activated sensors. Phototoxicity graphs are from three replicates and show mean and standard deviation.

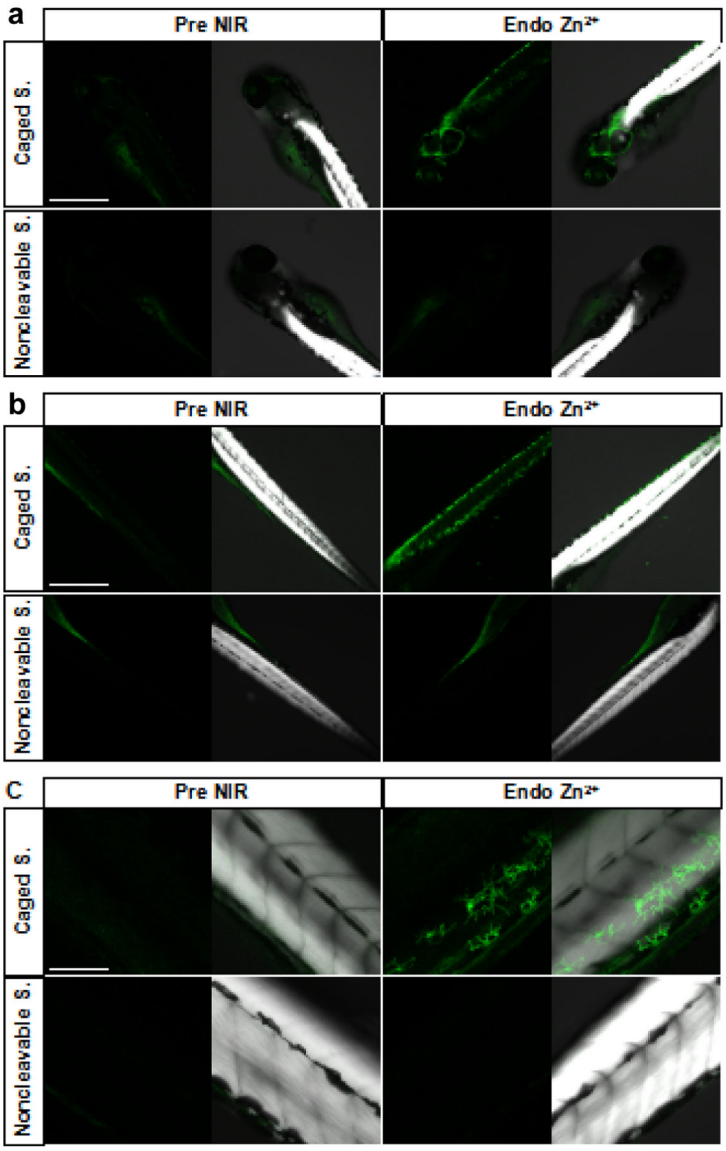

Figure 5:

In vivo Zn^{2+} detection in 3 days post fertilization (dpf) larvae by NIR photoactivation sensor. (a–c) Representative confocal images of Zn^{2+} detection by the Zn^{2+} sensor in zebrafish 3 dpf larvae. Common gut autofluorescence are detected from control groups. Consistent with early embryo data, an increase of fluorescence signal in response to endogenous Zn^{2+} was observed in the head region (a) and some multidendritic pattern (as shown in panel c with higher magnitude) in the body region (b). No signal increase was observed from control groups using a non-cleavable inactive substrate strand in the sensor. Scale bar: 500 μm in (a) and (b); 100 μm in (c). “Pre NIR” groups show the background fluorescence signal. “Endo Zn^{2+}” groups show the fluorescence generated under endogenous Zn^{2+} from NIR-activated sensors.